 CMC, vol.1, no.4, pp.327-336, 2004

Lamb Wave Interaction with Delaminations in CFRP Laminates

Jiayong Tian[1,2], Ulrich Gabbert[2], Harald Berger[2], Xianyue Su[1]

Abstract: In this paper, we investigate Lamb wave interaction with delamination in an infinite carbon fiber reinforced plastics (CFRP) laminate by a hybrid method. The infinite CFRP laminate is divided into an exterior zone and an interior zone. In the exterior zone, the wave fields are expressed by wave mode expansion. In the interior zone, the wave fields are modeled by the finite element method (FEM). Considering the continuity condition at the boundary between the exterior and interior zones, the global wave fields can be calculated. Lastly, numerical examples show how a delamination in the laminate influences the mode conversion of different incident wave modes.

keyword: Lamb Wave, Delamination, CFRP Laminates, Finite Element Method, Wave Function Expansion

1 Introduction

Recently, considerable work has been focused on the development of smart structures. Smart structures can self-sense and self-process the environment information so that such structures offer new possibilities for a characterization of structures in the future. Carbon fiber reinforced plastics (CFRP) with surface bonded or embedded thin piezoceramic patches used as sensors and/or actuators are very attractive for designing smart structures. [Gabbert and Tzou (2001)] The main advantages of such structures are i) its light weight, high stiffness and high strength of material, which results from a tailored anisotropic layered design, and ii) its sensing and actuating capability which enables such structures to adaptively react to changing environmental conditions. But during manufacturing and also during operating such structures often inevitable imperfections can be observed in the smart piezoceramic CFRP laminates, such as local concentrations of fibers or epoxy, delaminations, debonding of active ceramics, local fiber cracks, voids, inclusion etc. [Pohl, Mook, and Michel (2000), Gabbert and Cao (1999)] In extension to conventional non-destructive evaluation methods (NDE), the smart material themselves can be used to monitor and to detect such damages and imperfections. Such real-time health monitoring techniques can increase the reliability of smart structures, reduce the operational costs and offer many unique opportunities to assess the structural integrity. There are some kinds of health monitoring method for smart piezoceramic CFRP laminates, such as electrical impedance spectroscopy, Lamb wave techniques etc. [Pohl, Mook, and Michel (2000)] From all of these methods, Lamb wave method seems to be the most attractive method for health monitoring in smart piezoceramic CFRP laminates. Lamb waves are one kind of guided waves that propagate in thin plates, which are also called plates modes. There are a finite number of symmetrical or anti-symmetric Lamb wave modes at a given frequency-thickness product, which are called S_0, S_1,..., S_n and A_0, A_1, ..., A_m. These Lamb waves modes have different phase velocity and group velocity. The integrated piezoceramic patches can actuate and sense ultrasonic Lamb waves propagating in the plane of CFRP laminates. The ultrasonic Lamb wave can propagate for a long distance so that the lamb wave method is suitable for global health monitoring of smart structures. Furthermore, ultrasonic Lamb waves are very sensitive to delamination, which are typical defects in smart CFRP laminates. [Kundu, Karpur, Matikas, and Nicolau (1996)] For quantitative evaluations by Lamb wave techniques, it is important to investigate Lamb wave interaction with delamination. As a first step in this paper infinite CFRP laminates are investigated.

The wave scattering due to defects in plates has received considerable attention in the literature. Pao and Mow [Pao and Mow (1973)] used the wave function expansion method to investigate the diffraction of elastic wave by a circular hole in an infinite isotropic plate. But the wave function expansion method is only suit-

[1] Department of Mechanics and Engineering Science, Peking University, Beijing, 100871, P.R.China
[2] Institute of Mechanics, Otto-Von-Guericke University, Magdeburg, 39106, Germany

able for simple boundaries, such as circular or elliptical holes etc. Abduljabbar [Abduljabbar, Datta, and Shah (1983)] presented a hybrid method combining the finite element method and the wave expansion method to solve the scattering of SH waves by arbitrarily shaped cracks in isotropic plates. Doyle [Doyle (1997)] presented the spectral super-element method, which is similar with the hybrid method presented by Abduljabbar, [Abduljabbar, Datta, and Shah (1983)] to analyze the incident longitudinal wave interaction with a transverse crack in a plate. Karumasena et al. [Karunasena, Liew, and Kitipornchai (1995)] extended the hybrid method to investigate the wave scattering by normal edge cracks in composite plates. Up to now, the investigation of Lamb wave reflections and transmissions caused by delaminations in CFRP laminates has not been reported in literatures.

In the paper the Lamb wave interaction with a delamination in an infinite CFRP laminate is investigated by the hybrid method combining analytical and numerical methods. For this purpose the infinite CFRP laminate is divided into two zones, which are called exterior zone and the interior zone. In the exterior zone wave fields are expressed analytically by the wave mode expansion method. In the interior zone, the wave field is approximated by the finite element method. Taking into account the continuity conditions at the boundaries between the exterior and interior zones, the global wave fields can be calculated. Lastly, numerical examples are presented to show the delamination influences the mode conversion of the different incident wave modes. The numerical results may be helpful to better understand and to apply the Lamb wave techniques experimentally to monitor the integrity of smart piezoceramic structures.

2 The Hybrid Method

Consider an infinite CFRP laminate consisting of several unidirectional fibrous composites laminaes of the same material rigidly bonded at their interfaces, combinations of only 0° and 90° layups are allowed. Here one global coordinate system with the origin at the upper surface of CFRP laminate are introduced, where x coincides with the fiber direction of upper surface of the CFRP laminate and y coincide with the thickness direction of laminate. In the following the hybrid method is presented to analyze the reflection and the transmission of harmonic plane strain waves if delaminations occurs in CFRP laminates. Here it is assumed that delamination of length a is located at $x=0$, $y=y_0$ in the CFRP laminate (see Fig.1). The incident Lamb wave propagates from $x=\infty$ along the negative x axis. The laminate is divided into two types of zones: i) the exterior zones A and B which includes the reflected wave zone and the transmitted wave zone, and ii) the interior zone of length (x_1+x_2), where x_1 and x_2 are greater than one half of the delamination length a.

2.1 Wave function expansion in the exterior zone of the CFRP laminate

2.1.1 The reflected wave zone and the incident wave zone

In the exterior zone of the CFRP laminate we consider that the laminate consists of several unidirectional laminaes, each laminae is modeled as an orthrotropic material. In each laminae, the constitutive equation is given by

$$\begin{bmatrix} \sigma_{xx} \\ \sigma_{yy} \\ \sigma_{xy} \end{bmatrix} = \begin{bmatrix} C_{11} & C_{12} & C_{13} \\ C_{21} & C_{22} & C_{23} \\ C_{31} & C_{32} & C_{33} \end{bmatrix} \begin{bmatrix} \varepsilon_{xx} \\ \varepsilon_{yy} \\ \gamma_{xy} \end{bmatrix}, \tag{1}$$

where σ_{ij} and ε_{ij} are the stress and strain components. $\gamma_{xy}=2\varepsilon_{xy}$. The strain is denoted by

$$\varepsilon_{xx}=\frac{\partial u_x}{\partial x}, \varepsilon_{yy}=\frac{\partial u_y}{\partial y}, \gamma_{xy}=\frac{\partial u_x}{\partial y}+\frac{\partial u_y}{\partial x}, \tag{2}$$

where u_x and u_y are the displacement components along the x and the y axis, respectively, which satisfy the motion equations.

$$C_{11}\frac{\partial^2 u_x}{\partial x^2}+C_{22}\frac{\partial^2 u_x}{\partial x^2}+(C_{12}+C_{33})\frac{\partial^2 u_y}{\partial x \partial y}=\rho\frac{\partial^2 u_x}{\partial t^2}, \tag{3}$$

$$(C_{12}+C_{33})\frac{\partial^2 u_x}{\partial x \partial y}+C_{22}\frac{\partial^2 u_y}{\partial y^2}+C_{33}\frac{\partial^2 u_y}{\partial x^2}=\rho\frac{\partial^2 u_y}{\partial t^2}. \tag{4}$$

Formal solutions for the motion equations can be sought in the following form

$$(u_x,u_y)=\sum_{q=1}^{4}(1,W_q)U_{1q}e^{ik(x+\alpha_q y)-i\omega t}, \tag{5}$$

where $i=\sqrt{-1}$, k is the x component of the wave number, ω is the circular frequency, α is an ratio of the wave number components along the y and x direction which can be derived from Eq. (3) and (4), U_1 is the unknown

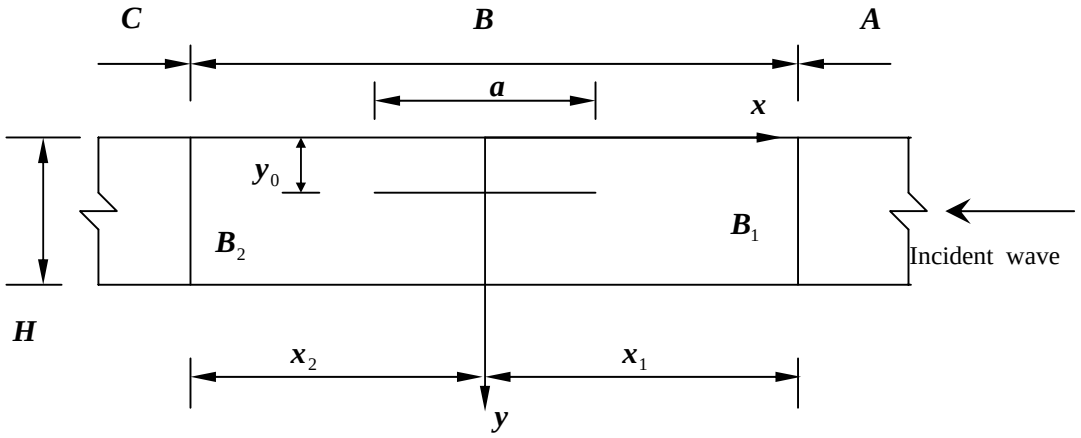

Figure 1 : Delamination of composite laminate

amplitude of displacement u_x, W is the ratio of the amplitude of displacement u_y and u_x.

Assumed that the interface between the different laminaes is rigidly and bonded and the both surfaces of CFRP laminate is traction free and adopting the global matrix formulation [Lowe (1995)] for the infinite CFRP laminate and the eigenvalue problem can be written as

$$[\mathbf{K}]\,\mathbf{Q} = \mathbf{0}, \tag{6}$$

where $\mathbf{Q} = \left[\mathbf{U}_1^1, \mathbf{U}_1^2, ...\mathbf{U}_1^n\right]^T$ is the amplitude vector of displacement u_x of CFRP laminate.

If $\mathbf{Q}$ has non-trivial solution, the determinant of $[\mathbf{K}]$ must be zero. The solution of the eigenvalue problems results in the different wave numbers k_i and the corresponding displacement mode shape φ_i, where the real k_i represents the propagating Lamb wave modes and the non-real k_i represents the non-propagating Lamb wave modes.

To ensure that the reflected waves produce bounded displacements and stresses throughout the CFRP laminate, the admissible wave numbers k must be those real roots with positive group velocity and those non-real roots with $Im(k) > 0$. A total of M number of roots k are ordered as follows: real roots are ordered firstly in decreasing order of their magnitude; non-real roots are ordered next in the ascending order of magnitude of their imaginary parts. If a complex k is encountered, which is not purely imaginary, the negative complex conjugate $-\overline{k}$ is also included.

The reflected waves in the zone A (see Fig. 1) can be approximately expressed by a summation of the first $M1$ Lamb wave modes.

$$\mathbf{q}^r(x,y) = \sum_{m=1}^{M1} A_m \varphi_{\mathbf{m}}(k_m, y)\exp(ik_m x)\exp(-i\omega t), \quad x > x_1, \tag{7}$$

where A_m is the magnitude of the mth reflected wave mode, $\mathbf{q}^r(x,y) = [u_x(x,y), u_y(x,y)]^T$ is the displacement vector, $\varphi_{\mathbf{m}}$ is the m^{th} displacement mode shape of the corresponding displacement. The factor $\exp(-i\omega t)$ is omitted in the following analysis.

The stress components in the infinite CFRP laminate caused by the reflected waves are denoted by

$$\mathbf{p}^r(x,y) = \sum_{m=1}^{M1} A_m \psi_{\mathbf{m}}(k_m, y)\exp(ik_m x), \quad x > x_1, \tag{8}$$

where $\mathbf{p}^r(x,y) = [\sigma_{xx}(x,y), \sigma_{xy}(x,y)]^T$ is the stress vector, $\sigma_{xx}(x,y)$ and $\sigma_{xy}(x,y)$ are the stresses along the x and y axis, respectively, $\psi_m(k_m, y)$ is the m^{th} stress mode shape of the corresponding stresses.

After discretization along the boundary B_1, the boundary displacements of the reflected wave can be expressed approximately by the nodal displacements as

$$\mathbf{q}^r(x_1, y) = \mathbf{N}\mathbf{Q}^r(x_1), \tag{9}$$

where $\mathbf{N}$ is shape function, which is determined by the finite element type used in the interior zone, and $\mathbf{Q}^r(x_1) = \left[\ \mathbf{q}^r(x_1,y_1)^T \quad \mathbf{q}^r(x_1,y_2)^T \quad \cdots \quad \mathbf{q}^r(x_1,y_{N1})^T\ \right]$ is the vector of the nodal displacements along the boundary B_1, which can be expressed as

$$\mathbf{Q}^r(x_1) = \mathbf{G_1}\mathbf{D_1}(x_1), \tag{10}$$

with

$$\mathbf{G}_1 = \begin{bmatrix} \varphi_1(k_1,y_1) & \varphi_2(k_1,y_1) & \cdots & \varphi_{M1}(k_1,y_1) \\ \varphi_1(k_1,y_2) & \varphi_2(k_1,y_2) & \cdots & \varphi_{M1}(k_1,y_2) \\ \vdots & \vdots & \ddots & \vdots \\ \varphi_1(k_1,y_{N1}) & \varphi_2(k_1,y_{N1}) & \cdots & \varphi_{M1}(k_1,y_{N1}) \end{bmatrix}$$

and $\mathbf{D}_1(x) =$
$[\, A_1\exp(ik_1x_1) \;\; A_2\exp(ik_2x_1) \;\; \cdots \;\; A_{M1}\exp(ik_{M1}x_1) \,]^T$.
The forces at boundary nodes are denoted by

$$\mathbf{P}^r(x_1) = \mathbf{F}_1\mathbf{D}_1(x_1), \tag{11}$$

where $\mathbf{P}^r(x_1) =$
$[\, \mathbf{F}^r(x_1,y_1)^T \;\; \mathbf{F}^r(x_1,y_2)^T \;\; \cdots \;\; \mathbf{F}^r(x_1,y_{N1})^T \,]^T$
is the nodal force vector along the boundary B_1, with

$$\mathbf{F}_1 = \left[\int_{B_1} \mathbf{N}\psi_1(k_1,y_1)\,dy \;\; \int_{B_1} \mathbf{N}\psi_2(k_2,y_2)\,dy \;\; \cdots \;\; \int_{B_1} \mathbf{N}\psi_{M1}(k_{M1},y_{N1})\,dy \right].$$

The displacements and forces at boundary nodes for the p^{th} incident wave can be expressed by

$$\mathbf{Q}^{in}(x_1) = A_p^{in}\mathbf{G}_{1p}(-k_p)\exp(-ik_px_1), \tag{12}$$

$$\mathbf{P}^{in}(x_1) = A_p^{in}\mathbf{F}_{1p}(-k_p)\exp(-ik_px_1), \tag{13}$$

where $\mathbf{G}_{1p}$ and $\mathbf{F}_{1p}$ are the p^{th} column of $\mathbf{G}_1$ and $\mathbf{F}_1$, respectively, after replacing the wave number k_p by its negative value.

2.1.2 The transmitted wave zone

The transmitted wave in zone C can also be written in the above given form as

$$\mathbf{q}^t(x,y) = \sum_{m=1}^{M2} B_m\varphi_{\mathbf{m}}(-k_m,y)\exp(-ik_mx), \quad x < x_2. \tag{14}$$

After discretization along the boundary B_2, the displacements and forces at the boundary nodes are written as

$$\mathbf{Q}^t(x_2) = \mathbf{G}_2\mathbf{D}_2(x_2), \tag{15}$$

$$\mathbf{P}^t(x_2) = \mathbf{F}_2\mathbf{D}_2(x_2), \tag{16}$$

with $\mathbf{Q}^t(x) =$
$[\, \mathbf{q}^t(x_2,y_1)^T \;\; \mathbf{q}^t(x_2,y_2)^T \;\; \cdots \;\; \mathbf{q}^t(x_2,y_{N2})^T \,]$,
$\mathbf{G}_2 =$

$$\begin{bmatrix} \varphi_1(-k_1,y_1) & \varphi_2(-k_1,y_1) & \cdots & \varphi_{M2}(-k_1,y_1) \\ \varphi_1(-k_1,y_2) & \varphi_2(-k_1,y_2) & \cdots & \varphi_{M2}(-k_1,y_2) \\ \vdots & \vdots & \ddots & \vdots \\ \varphi_1(-k_1,y_{N2}) & \varphi_2(-k_1,y_{N2}) & \cdots & \varphi_{M2}(-k_1,y_{N2}) \end{bmatrix},$$

$$\mathbf{F}_2 = \left[\int_{B_2} \mathbf{N}\psi_1(k_1,y_1)\,dy \;\; \int_{B_2} \mathbf{N}\psi_2(k_2,y_2)\,dy \;\; \cdots \;\; \int_{B_2} \mathbf{N}\psi_{M2}(k_{M2},y_{N2})\,dy \right],$$

$$\mathbf{D}_2(x) = [B_1\exp(ik_1x_2) \;\; B_2\exp(ik_2x_2) \;\; \cdots \;\; B_{M2}\exp(ik_{M2}x_2)]^T.$$

2.2 Finite element approximation of the interior zone

Because of complicated geometry, the wave fields in the interior zone B containing the delamination are difficult to express by wave functions. One of significant advantages of the conventional finite element is their modeling of the complicated geometries. So the finite element method is applied to model the wave fields in the interior zone. In this paper the delamination is assumed to be a crack with traction free surfaces. According to the virtual work principle the finite element approximation results in the following formulation

$$\delta\overline{\mathbf{Q}}^{\mathbf{T}}[\mathbf{S}]\mathbf{Q} - \delta\overline{\mathbf{Q}}_{\mathbf{B}}^{\mathbf{T}}\mathbf{P}_{\mathbf{B}} = 0, \tag{17}$$

where $\mathbf{Q}^T = \left[\mathbf{Q}_I^T, \mathbf{Q}_{B_1}^T, \mathbf{Q}_{B_2}^T\right]^T$ is the global nodal displacement vector, $\mathbf{Q}_I$ is the interior nodal displacement vector, $\mathbf{Q}_{B_1}$ and $\mathbf{Q}_{B_2}$ are the nodal displacement vectors along the boundary B_1 and B_2, respectively, $\mathbf{P}_B^T = \left[\, \mathbf{P}_{B_1}^T \;\; \mathbf{P}_{B_2}^T \,\right]^T$ is the nodal force vector at the boundary B_1 and B_2, and the matrix $\boldsymbol{S}$ is written as

$$\mathbf{S} = \mathbf{K} - \omega^2\mathbf{M} = \begin{bmatrix} \mathbf{S}_{II} & \mathbf{S}_{IB_1} & \mathbf{S}_{IB_2} \\ \mathbf{S}_{B_1I} & \mathbf{S}_{B_1B_1} & \mathbf{S}_{B_1B_2} \\ \mathbf{S}_{B_2I} & \mathbf{S}_{B_2B_1} & \mathbf{S}_{B_2B_2} \end{bmatrix}$$

with the global stiffness matrix $\mathbf{K}$ and the global mass matrix $\mathbf{M}$ of the finite-element-discretized interior zone,

respectively. With $\mathbf{S}$, Eq. (14) can be written as

$$\mathbf{S}_{II}\mathbf{Q}_I + \mathbf{S}_{IB_1}\mathbf{Q}_{B_1} + \mathbf{S}_{IB_2}\mathbf{Q}_{B_2} = 0, \tag{18}$$

$$\mathbf{S}_{IB_1}\mathbf{Q}_I + \mathbf{S}_{B_1B_1}\mathbf{Q}_{B_1} + \mathbf{S}_{B_1B_2}\mathbf{Q}_{B_2} = \mathbf{P}_{B_1}, \tag{19}$$

$$\mathbf{S}_{IB_2}\mathbf{Q}_I + \mathbf{S}_{B_2B_1}\mathbf{Q}_{B_1} + \mathbf{S}_{B_1B_2}\mathbf{Q}_{B_2} = \mathbf{P}_{B_2}. \tag{20}$$

2.3 The Global solution

Considering the following boundary condition at the boundary B_1 and B_2, respectively,

$$\mathbf{Q}_{B_1} = \mathbf{Q}^{in}(x_1) + \mathbf{Q}^{r}(x_1), \tag{21}$$

$$\mathbf{P}_{B_1} = \mathbf{P}^{in}(x_1) + \mathbf{P}^{r}(x_1), \tag{22}$$

$$\mathbf{Q}_{B_2} = \mathbf{Q}^{t}(x_2), \tag{23}$$

$$\mathbf{P}_{B_2} = -\mathbf{P}^{t}(x_2) \tag{24}$$

and substitution of Eqs. (10-11),(15-16), and (21-24) into (18-20) yields

$$\mathbf{A}_{11}\mathbf{D}_1(x_1) + \mathbf{A}_{12}\mathbf{D}_2(x_2) = \mathbf{C}_1, \tag{25}$$

$$\mathbf{A}_{21}\mathbf{D}_1(x_1) + \mathbf{A}_{22}\mathbf{D}_2(x_2) = \mathbf{C}_2, \tag{26}$$

with

$$\mathbf{A}_{11} = \left[\mathbf{S}_{B_1B_1} - \mathbf{S}_{B_1I}(\mathbf{S}_{II})^{-1}\mathbf{S}_{IB_1}\right]\mathbf{G}_1 - \mathbf{F}_1,$$

$$\mathbf{A}_{12} = \left[\mathbf{S}_{B_1B_2} - \mathbf{S}_{B_1I}(\mathbf{S}_{II})^{-1}\mathbf{S}_{IB_2}\right]\mathbf{G}_2,$$

$$\mathbf{A}_{21} = \left[\mathbf{S}_{B_2B_1} - \mathbf{S}_{B_2I}(\mathbf{S}_{II})^{-1}\mathbf{S}_{IB_1}\right]\mathbf{G}_1,$$

$$\mathbf{A}_{22} = \left[\mathbf{S}_{B_2B_2} - \mathbf{S}_{B_2I}(\mathbf{S}_{II})^{-1}\mathbf{S}_{IB_2}\right]\mathbf{G}_2 + \mathbf{F}_2,$$

$$\mathbf{C}_1 = \mathbf{P}^{in}(x_1) - \left[\mathbf{S}_{B_1B_1} - \mathbf{S}_{B_1I}(\mathbf{S}_{II})^{-1}\mathbf{S}_{IB_1}\right]\mathbf{Q}^{in}(x_1),$$

$$\mathbf{C}_2 = \left[\mathbf{S}_{B_2B1} - \mathbf{S}_{B_2I}(\mathbf{S}_{II})^{-1}\mathbf{S}_{IB_1}\right]\mathbf{Q}^{in}(x_1),$$

which can be written in a short form as

$$\mathbf{AD} = \mathbf{C} \tag{27}$$

with

$$\mathbf{A} = \begin{bmatrix} \mathbf{A}_{11} & \mathbf{A_{12}} \\ \mathbf{A_{21}} & \mathbf{A}_{22} \end{bmatrix},$$

$$\mathbf{D}^T = \begin{bmatrix} \mathbf{D}_1^T(x_1) & \mathbf{D}_2^T(x_2) \end{bmatrix}^T,$$

$$\mathbf{C}^T = \begin{bmatrix} \mathbf{C}_1^T & \mathbf{C}_2^T \end{bmatrix}^T.$$

After $\mathbf{D}$ is known by solving Eq.(27) the amplitudes A_m and B_m can be obtained from $\mathbf{D}_1(x_1)$ and $\mathbf{D}_2(x_1)$ in Eqs.(10) and (16).

2.4 The energy flux

The time average values of energy flux associated with the n^{th} reflected or m^{th} transmitted propagating Lamb wave mode through the cross section of the plate, caused by the p^{th} incident Lamb wave mode, can be defined as

$$I^r_{pn} = \omega|A_n|^2 \int_0^H Im(\psi_n(y)\overline{\varphi}_n(y))dy, \tag{28}$$

$$I^t_{pm} = \omega|B_m|^2 \int_0^H Im(\psi_m(y)\overline{\varphi}_m(y))dy, \tag{29}$$

$$I^{in}_{p} = \omega|A^{in}_p|^2 \int_0^H Im(\psi_p(y)\overline{\varphi}_p(y))dy. \tag{30}$$

Define the proportion of incident energy transferred into the n^{th} reflected Lamb wave mode and the m^{th} transmit Lamb wave mode E^r_{pn} and E^t_{pm} as

$$E^r_{pn} = I^r_{pn}/I^{in}_p, \tag{31}$$

$$E^t_{pm} = I^t_{pm}/I^{in}_p. \tag{32}$$

The percentage error in energy balance ε can be defined as

$$\varepsilon = 100\left(1 + \sum_n E^r_{pn} - \sum_m E^t_{pm}\right). \tag{33}$$

3 Examples

In the following, an infinite cross-ply $[0,90^\circ]_S$ CFRP laminate with a delamination, are used to test the above given approach. The cross-ply laminate has four layers. Each layer has the same thickness and material constants. The elastic constants of each of the layers of the laminate [Nayfeh (1995)] are

$$C_{11}/C_{33} = 155.43/7.48,$$

$$C_{12}/C_{33} = 3.72/7.48,$$

$$C_{13} = C_{23} = 0,$$

$$C_{22}/C_{33} = 16.34/7.48.$$

The frequency and the wave number are normalized as

$$\Omega = \omega H \Big/ \sqrt{C_{33}/\rho}, \quad \mathrm{K} = kH,$$

where ρ is the density and H is the thickness of the CFRP laminate.

Table 1 : E^r_{pn} and E^t_{pm} and ε for the cross-ply laminate with delamination length a/H = 1 at $\Omega = 9.1$

y_0/H	p	E^r_{pm}						ε
		$1A$	$2A$	$3A$	$1S$	$2S$	$3S$	
0.5	$1A$	-0.0066	-0.0066	-0.0001	-0.0000	-0.0000	-0.0000	
	$2A$	-0.0051	-0.0184	-0.0018	-0.0000	-0.0000	-0.0000	
	$3A$	-0.0000	-0.0002	-0.0469	-0.0000	-0.0000	-0.0000	
	$1S$	-0.0000	-0.0000	-0.0000	-0.0295	-0.0082	-0.0033	
	$2S$	-0.0000	-0.0000	-0.0000	-0.0139	-0.0221	-0.0014	
	$3S$	-0.0000	-0.0000	-0.0000	-0.0049	-0.0027	-0.0255	
	p	E^t_{pm}						
	$1A$	0.9545	0.0175	0.0139	0.0000	0.0000	0.0000	0.08
	$2A$	0.0199	0.8837	0.0673	0.0000	0.0000	0.0000	0.38
	$3A$	0.0149	0.0789	0.8653	0.0000	0.0000	0.0000	-0.63
	$1S$	0.0000	0.0000	0.0000	0.8983	0.0141	0.1030	-5.6
	$2S$	0.0000	0.0000	0.0000	0.0119	0.8726	0.0854	-0.72
	$3S$	0.0000	0.0000	0.0000	0.0266	0.0755	0.8438	2.1

For the finite element approximation of the interior zone, eight-node rectangular finite elements with quadratic shape functions are used. For the analysis the commercial available finite element software 'COSAR' was applied. [Berger, Gabbert, Köppe, and Seeger (2000), COSAR] Based on the substructure technique of this software the systems matrices of the boundary nodes are calculated. These matrices are available via a data interface for any application outside the finite element software.

4 Computational Results

The dispersion curves for the cross-ply laminate are shown in Fig.2. The solid line and the dash line represent the anti-symmetric Lamb wave mode and symmetric Lamb wave mode, respectively.

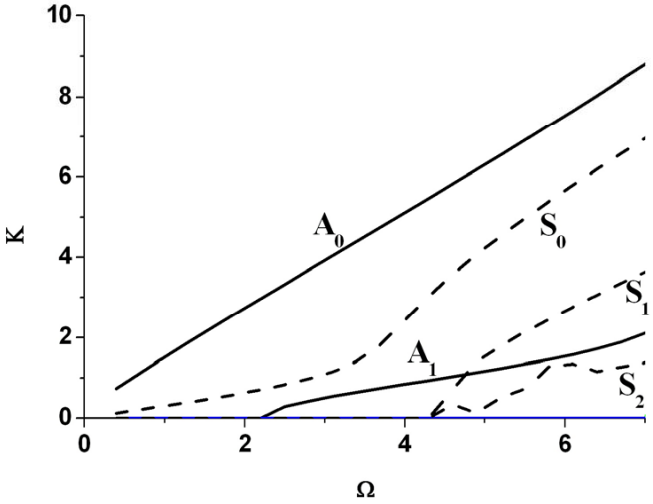

Figure 2 : Dispersive curve for CFRP laminate

In order to verify the accuracy of the numerical calculation a test case with a delamination length $a = 0$ in Zone B is calculated firstly for the cross-ply laminates. Because there is no defect in the laminates, the incident Lamb wave will be transmitted completely without any reflection. The maximum computational error of $|1 - E^t_{nn}|$ is less than 0.1%. Table 1 show E^r_{pn} and E^t_{pm} and the percentage error ε for cross-ply laminate respectively at $\Omega = 9.1$. Because of the structural symmetry with respect to the middle plane of laminate, Table 1 indicates that there is no coupling between the symmetric Lamb wave mode and the anti-symmetric Lamb wave mode. The maximum error ε for the cross-ply laminate is 5.6% . It is also concluded from Table 1 that E^r_{pn} and E^t_{pm} satisfy the reciprocity relation [Karunasena, Liew, and Kitipornchai (1995)] within the small errors, which results in

$$E^r_{pn} = E^r_{np}, \quad E^t_{pm} = E^t_{mp}.$$

Figure 3 shows E^r_{11}, E^t_{11}, $E^r_{1^*}$, and $E^t_{1^*}$ for the different delamination length in the cross-ply CFRP laminate with $y_0/H = 0.5$. Here $p,n,m = 1$ represents the A_0 mode

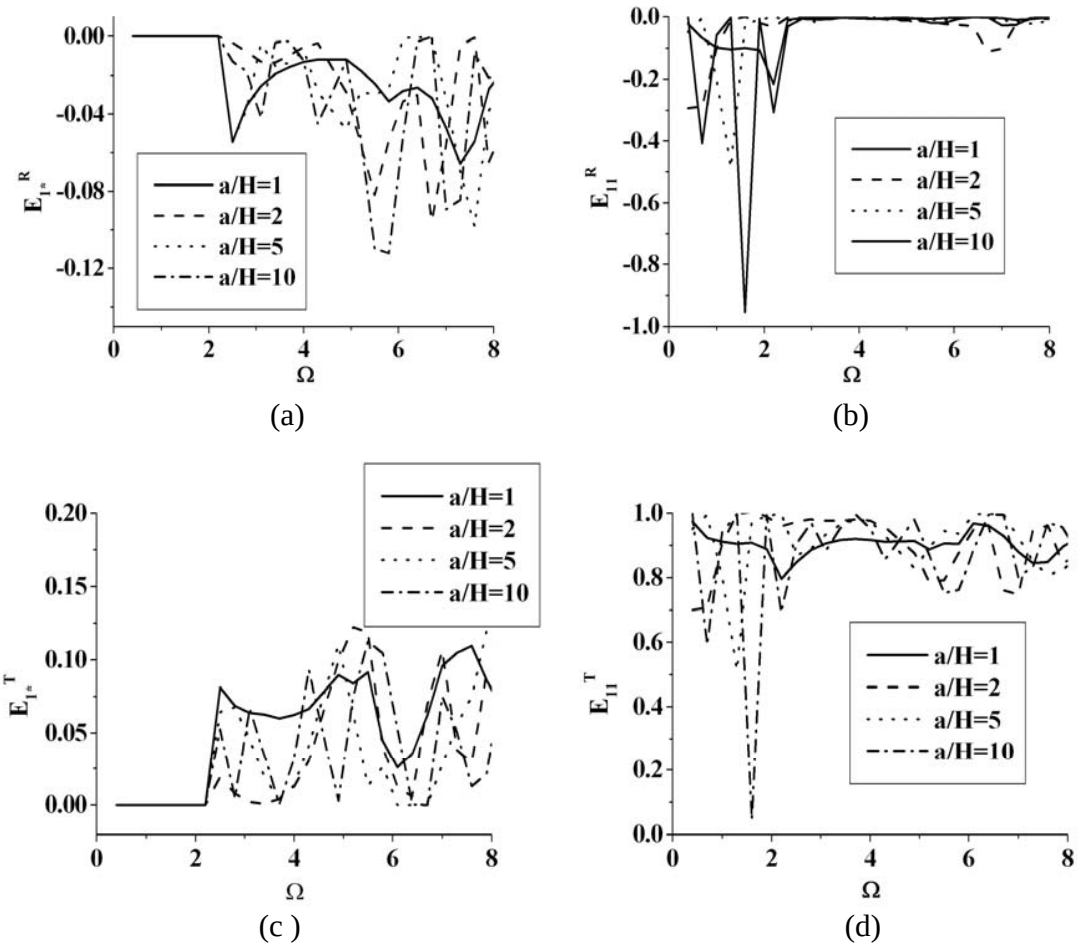

Figure 3 : Proportions of energy for the first incident antisymmetric lamb wave for different delamination length in crossply CFRP laminate

of Lamb waves, and $p,n,m = 2$ represents the S_0 mode of Lamb waves and E_{p^*} is the sum of the proportion of the p^{th} incident energy transferred into the other higher Lamb wave mode except A_0 and S_0. Four cases for the delamination length $a/H = 1$, $a/H = 2$, $a/H = 5$, and $a/H = 10$ are considered here. Figures show that until Ω reaches the cut-off frequency Ω_{A1} of A_1 mode of Lamb waves, there is much more reflection for the four cases for the incident A_0 mode of Lamb waves. Especially for $a/H = 1.0$ of the delamination length, nearly 95 percent of incident Lamb wave energy is transfer are transferred into the reflected A_0 mode at a specific frequency range. But after Ω reaches the cut-off frequency of the A_1 mode of Lamb waves, little reflection exists for four cases of delamination length and nearly all of energy is transferred into the transmitted lamb wave. Most of the transmitted lamb wave energy is focused on the A_0 mode and other energy will be transferred into the higher anti-symmetric lamb wave mode. From the above, it is concluded that the frequency range $[0,\Omega_{A1}]$, is sensitive to delamination for the incident A_0 mode.

E^r_{22} , E^t_{22} , $E^r_{2^*}$, and $E^t_{2^*}$ for the different delamination length in the cross-ply CFRP laminate with $y_0/H = 0.5$ are shown in Fig. 4. It is seen from Fig.4 that when the frequency is smaller than the cut off frequency Ω_{s1} of the S_1 mode of Lamb waves, all of the incident S_0 lamb wave will be transferred into the transmitted S_0 Lamb wave. When the frequency is greater than Ω_{s1}, there will be strong reflection for the incident S_0 Lamb wave and nearly 40 percent energy will be transmitted into higher symmetric Lamb wave in some frequency range. That is to say, the incident S_0 Lamb wave is sensitive to delamination only when the frequency is

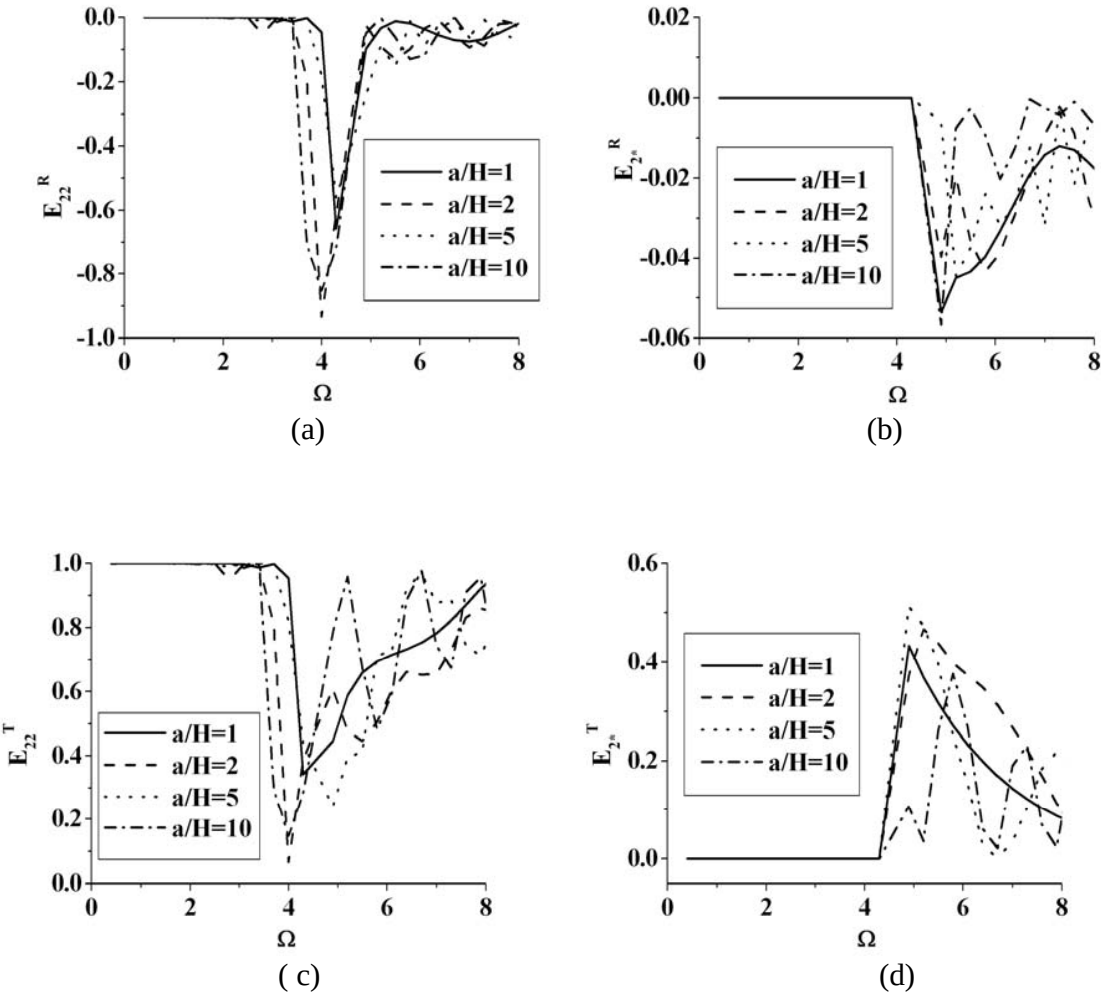

Figure 4 : Proportions of energy for the first incident symmetric lamb wave for different delamination length in crossply CFRP laminate

greater than Ω_{s1}.

E_{11}^r, E_{11}^t, E_{12}^r, and E_{12}^t for the different delamination position in the cross-ply CFRP laminate with $a/H = 1$ are shown in Fig.5 respectively. Here the two cases $y_0/H = 0.5$ and $y_0/H = 0.75$, are only considered. That is to say, one delamination is in the interface between the second layer and third layer and the other is in the interface between the first layer and the second layer. Because of non-symmetry for delamination position $y_0/H = 0.75$, it is seen that some energy of the incident A_0 lamb wave is not transferred into symmetric lamb wave mode until the frequency reaches Ω_{A1}. Especially in the higher frequency, more energy of the incident A_0 lamb wave is transferred into the transmitted S_0 mode. So the delamination position influences greatly the mode conversion.

Figure 6 shows E_{21}^r E_{22}^r, E_{21}^t, and E_{22}^t for the different delamination position in the cross-ply CFRP laminate with $a/H = 1$. Compared with Fig.5, it indicates that E_{12}^r, E_{21}^r and E_{21}^t, E_{12}^t satisfy the reciprocity relation, so the similar result about mode conversion with the incident A_0 lamb wave can be given.

5 Conclusion

In the paper, Lamb wave interaction with delamination in an infinite CFRP laminate has been investigated by a hybrid method combining the finite element method with wave mode expansion method. Numerical results indicate that the A_0 mode of Lamb wave is sensitive to the

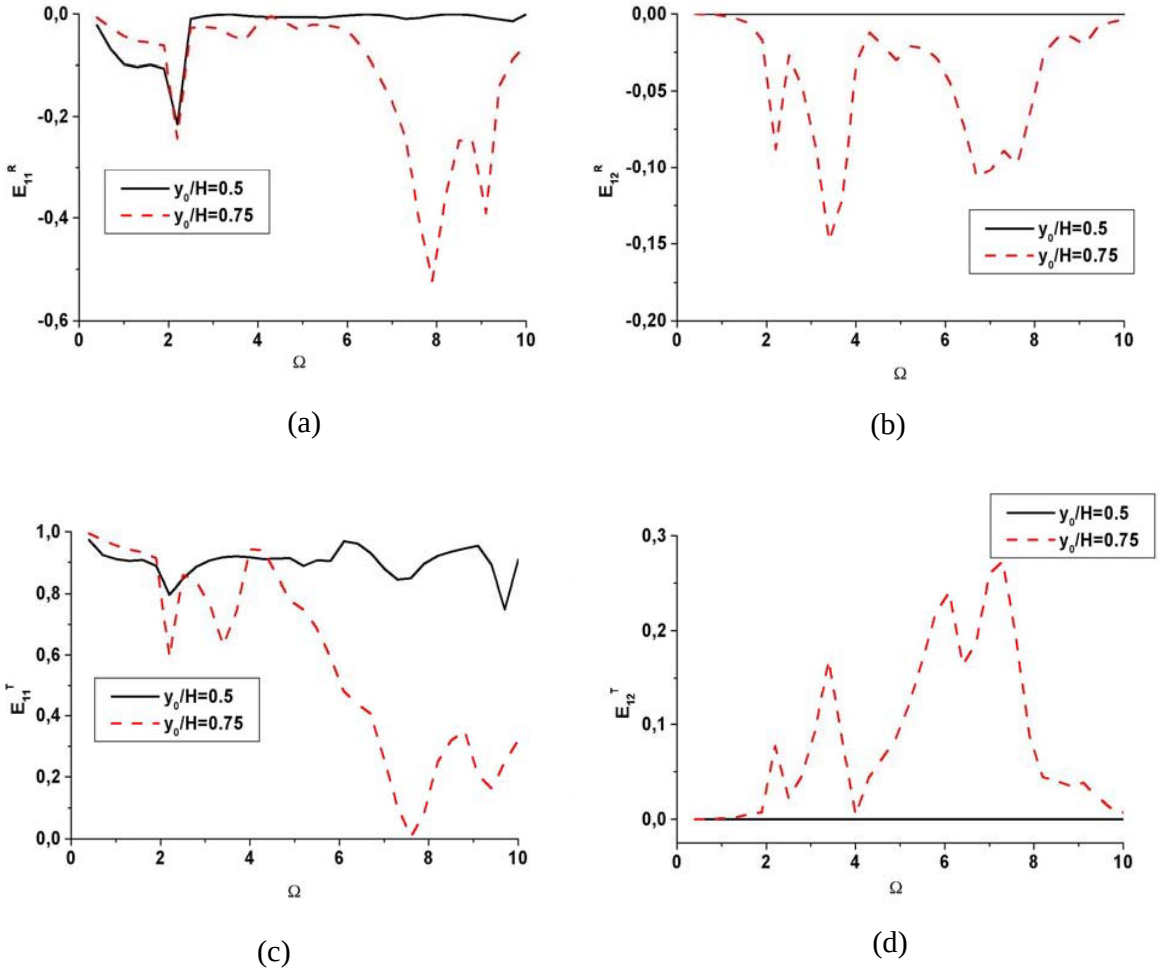

Figure 5 : Proportions of energy for the first incident antisymmetric lamb wave for different delamination position in crossply CFRP laminate

delamination in the frequency range $[0, \Omega_{A1}]$ and the S_0 mode of lamb wave is sensitive to the delamination when the frequency is greater than the frequency Ω_{s1}. The delamination position influences greatly the mode conversion for the antisymmetric Lamb wave and symmetric Lamb wave. The results show the potential applications of Lamb wave techniques in health monitoring of smart piezoelectric CFRP laminates. The continuation of this work intends to investigate the Lamb wave propagation in smart CFRP laminates actuated by surface or embedded piezoceramics by hybrid methods.

Acknowledgement: This first author would like to acknowledge the supports from Gottlieb Daimler and Karl Benz Foundation under the Stipendienprogramm *Gottlieb Daimler and Karl Benz Foundation Fellowships for Ph.D. Students of Peking University* (Project Nr. 17-03/00) and from *the National Natural Science Foundation of China* (No. 10172004).

References

Abduljabbar, Z.; Datta, S. K.; Shah, A. H. (1983): Diffraction of horizontally polarized shear waves by normal edge cracks in a plate, *Journal of Applied Physics*, **54**, 461-472.

Berger, H.; Gabbert, U.; Köppe, H.; Seeger, F. (2000): Finite Element Analysis and Design of Piezoelectric Controlled Smart Structures. *Journal of Theoretical and Applied Mechanics,* **38**, 475-498

COSAR – General Purpose Finite Element Package, FEMCOS Magdeburg, see http://www.femcos.de.

Doyle, J. F. (1997): Wave propagation in structures: Spectral analysis using Fast discrete Fourier transform, Springer-Verlag New York, Inc., New York.

Gabbert, U.; Cao, X. (1999): Finite element analysis of fracture behaviour of piezoelectric smart materials. *International Journal of Materials & Product Technology*, **14**, 304-319

Gabbert, U.; Tzou, H. S. (Eds.) (2001): Smart Structures and Structronic Systems. Kluwer Academic Publishers, Dordrecht, Netherlands.

Karunasena, W. M.; Liew, K. M.; Kitipornchai, S. (1995): Hybrid analysis of Lamb wave reflection by a crack at the fixed edge of a composite plate, *Computer Methods in Applied Mechanics and Engineering*, **125**, 221-234.

Kundu, T.; Karpur, P.; Matikas, T.; Nicolau, P. (1996): Lamb wave mode sensitivity to detect various material defects in multilayered composite plates, *Review of Progress in Quantitative Nondestructive Evaluation, Vol. 15, Edited by D.O. Thompson and D.E. Chimenti*, Plenum Press, New York, 231-238.

Lowe, M. J. S. (1995): Matrix techniques for modeling ultrasonic waves in multi-layered Media, *IEEE Transactions on Ultrasonics, Ferroelectrics, and Frequency Control*, 42(4), 525-542.

Nayfeh, A. H. (1995): Wave propagation in layered anisotropic media with applications to composites, Elsevier, New York.

Pao, Y. H.; Mow, C.C. (1973): The diffraction of elastic waves and dynamics stress concentration, Crane, Russack and Company Inc., New York.

Pohl, J.; Mook, G.; Michel, F. (2000): Health monitor of smart CFRP-Structures, Proceeding of 15th World Conference on Non-destructive Testing, Roma, 380-383.